Article

Wybutosine hypomodification of tRNAphe activates HERVK and impairs neuronal differentiation

Chuanbo Sun,
Ruirui Guo,
Xiangyan Ye, ...,
Dengna Zhu,
Kaishou Xu, Hao
Hu

zhudengna@126.com (D.Z.)
xksyi@126.com (K.X.)
huh@cougarlab.org (H.H.)

Highlights

Translation efficiency of
UUU codon was
compromised in TYW1⁻/⁻
cells

Neuron differentiation was
impaired when TYW1 was
depleted

HERVK was elevated due
to reduced expression of
UUU codon-rich protein
SMARCAD1

Replenishment of
SMARCAD1 improved
neuron differentiation

iScience

CellPress
OPEN ACCESS

Article

Wybutosine hypomodification of tRNAphe activates HERVK and impairs neuronal differentiation

Chuanbo Sun,[1,8] Ruirui Guo,[2,3,8] Xiangyan Ye,[1,8] Shiyi Tang,[2] Manqi Chen,[2] Pei Zhou,[1] Miaomiao Yang,[1] Caihua Liao,[1] Hong Li,[1] Bing Lin,[1] Congwen Zang,[1] Yifei Qi,[1] Dingding Han,[1,4] Yi Sun,[5] Na Li,[1] Dengna Zhu,[6,*] Kaishou Xu,[7,*] and Hao Hu[1,6,9,*]

SUMMARY

We previously reported that loss of function of TYW1 led to cerebral palsy with severe intellectual disability through reduced neural proliferation. However, whether TYW1 loss affects neural differentiation is unknown. In this study, we first demonstrated that TYW1 loss blocked the formation of OHyW in tRNA[phe] and therefore affected the translation efficiency of UUU codon. Using the brain organoid model, we showed impaired neuron differentiation when TYW1 was depleted. Interestingly, retrotransposons were differentially regulated in TYW1^{−/−} hESCs (human embryonic stem cells). In particular, one kind of human-specific endogenous retrovirus-K (HERVK/HML2), whose reactivation impaired human neurodevelopment, was significantly up-regulated in TYW1^{−/−} hESCs. Consistently, a UUU codon-enriched protein, SMARCAD1, which was a key factor in controlling endogenous retroviruses, was reduced. Taken together, TYW1 loss leads to up-regulation of HERVK in hESCs by down-regulated SMARCAD1, thus impairing neuron differentiation.

INTRODUCTION

tRNAs must undergo extensive modifications before they can exert proper function. Either hyper- or hypomodifications of tRNAs lead to various disease states.[1] Importantly, the mutations of a number of tRNA enzymes have been revealed in neurological disease.[2–4] The modification of tRNA body, for example, at the D arm or T arm, may stabilize the tertiary structure of tRNAs. The modification of tRNA at wobble position (34 position) ensures exact codon-anticodon recognition, either restricting or expanding the decoding capacity of the tRNA.[5] Besides, modification at position 37 was believed to stabilize mRNA-tRNA interactions and thus ensured accurate decoding and reading frame maintenance in mRNA.[6]

We previously reported TYW1, a tRNA[phe] modification enzyme, regulates neural proliferation and migration during early neural development.[7] TYW1 catalyzes tricyclic ring formation from m1G at 37th position of tRNA[phe], which is a critical upstream process for OHyW formation.[8] Thus function loss of TYW1 may affect the accurate pairing of tRNA[phe] and its codons, leading to a low expression of phenylalanine-enriched proteins. During neural proliferation, several cell cycle-related proteins which enriched in phenylalanine were down-regulated in TYW1-knockout mice, thus restricting the proliferation rate.[7] The proper translation of proteins is not only important for proliferating neurons but also crucial for the maintenance of differentiation process, as translation profile is dynamically changed during brain development.[9] However, how TYW1 may regulate neuron differentiation is not known yet.

During neural development, neuron is differentiated from neural progenitors, a process which is precisely regulated by epigenetic programs.[10] Actually, in addition to protein-coding genes, the expression of noncoding sequences also regulates neural development.[11] The human genome contains ~45% transposon element; the expression of these transposon elements was well controlled by DNA methylation and histone modification.[12,13] Transposon elements are classified as DNA transposon or RNA transposon (retrotransposon). Long terminal repeat (LTR) transposon, representing transposons with long terminal repeats, was believed to be originated from exogenous infection by retrovirus during evolution, thus terming endogenous retrovirus (ERV). These transposons element was not recognized as "junk DNA" anymore; rather they regulated development and contributed to disease state, especially in neural system.[14,15] For example, human-specific transposon SINE-Vntr-Alus (SVAs) provided substrates for thousands of novel TBR2-binding sites.[16] LTR5_Hs may serve as antisense promoter

[1]Laboratory of Medical Systems Biology, Guangzhou Women and Children's Medical Center, Guangzhou Medical University, Guangzhou 510623, China
[2]Department of Histology and Embryology, Zhongshan School of Medicine, Sun Yat-sen University, Guangzhou 510275, China
[3]School of Basic Medical Science, Gansu Medical College, Pingliang 744000, Gansu, China
[4]Department of Clinical Laboratory, Shanghai Children's Hospital, School of Medicine, Shanghai Jiao Tong University, Shanghai 200062, China
[5]Department of Neonatology, Guangzhou Women and Children's Medical Center, Guangzhou Medical University, Guangzhou, Guangdong Province 510180, China
[6]Third Affiliated Hospital of Zhengzhou University, Zhengzhou 450052, China
[7]Department of Rehabilitation, Guangzhou Women and Children's Medical Center, Guangzhou Medical University, Guangzhou 510120, China
[8]These authors contributed equally
[9]Lead contact
*Correspondence: zhudengna@126.com (D.Z.), xksyi@126.com (K.X.), huh@cougarlab.org (H.H.)
https://doi.org/10.1016/j.isci.2024.109748
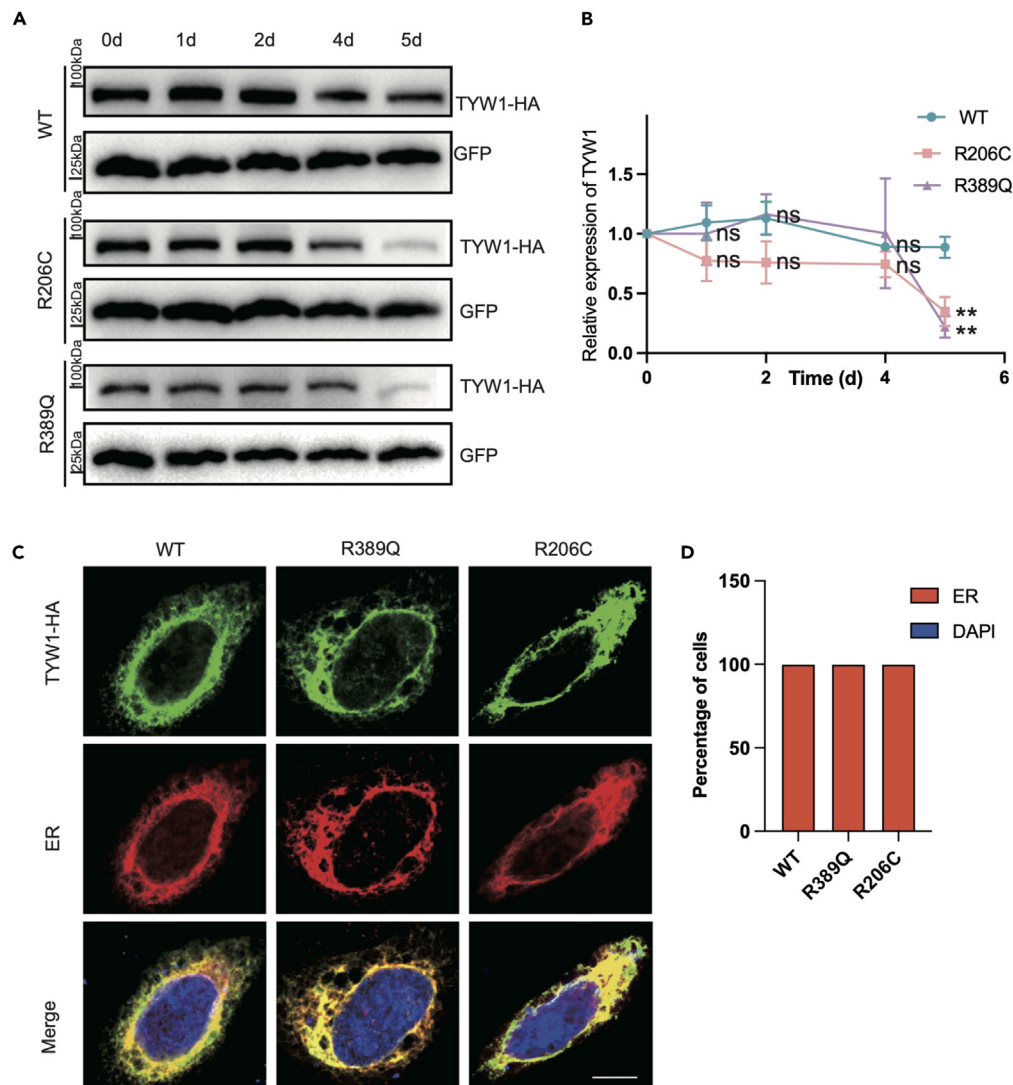
Figure 1. Variants of tRNA^phe modification enzyme TYW1 lead to decreased protein stability without changing subcellular localization

(A) Representative western blot image of cell lysates from HEK293 cells transfected with plasmids that expressed either wild-type TYW1 (WT), or with indicated variant types (R206C, R389Q). 0 day indicates the time when the cells were synchronized with cycloheximide.

(B) Line chart shows the relative expression of WT, R206C, R389Q at indicated time points after the cells were synchronized with cycloheximide. $n = 3$ independent replicates, data are presented as mean $\pm$ SD. $**p < 0.01$, ns, no significance from ordinary one-way ANOVA multiple comparisons within each time point.

(C) Immunostaining shows the subcellular localization of WT and mutated TYW1 protein in HeLa cells. Bar indicates 10 μm. ER, endoplasmic reticulum.

(D) Stacked bar plot show percentage of cells in which TYW1 colocalize with nucleus (DAPI) or cytoplasm (ER). 18 cells from each group from three independent experiments were analyzed. Pearson's_R value was calculated using colocalization finder of Fiji image tool. Pearson's_R > 0.5 was defined as colocalization.

to drive NTRK3 transcription.[17] ZNF417 and ZNF587 were dynamically expressed to control HERVK expression during human brain development.[18]

The regulation of LTR element by tRNA has long been noticed. In mouse embryonic stem (ES) cells and embryos, tRNA-Gly-GCC fragments regulated genes associated with murine endogenous retrovirus L (MERVL).[19] Recent studies revealed that mutation of NSUN2, a tRNA m5C methyltransferase, increased LTR transposon element expression by a mechanism related to tRNA stability and abundance.[20] Moreover, another study found the wobble U modifications by Elongator complex controlled the expression of TY1 elements as well as some endogenous genes associated with solo LTRs.[21] However, the mechanism was still mysterious. The control of tRNA on expression of LTR elements might rely on that tRNAs serve as primers for reverse transcriptase.[22,23] For example, tRFs (tRNA-derived fragments) were reported to inhibit LTR-retrotransposon by block reverse transcription and induction of RNAi in mouse ES cells.[24] Thus, it is interesting to explore how tRNA may regulate transposon expression under different modification states.
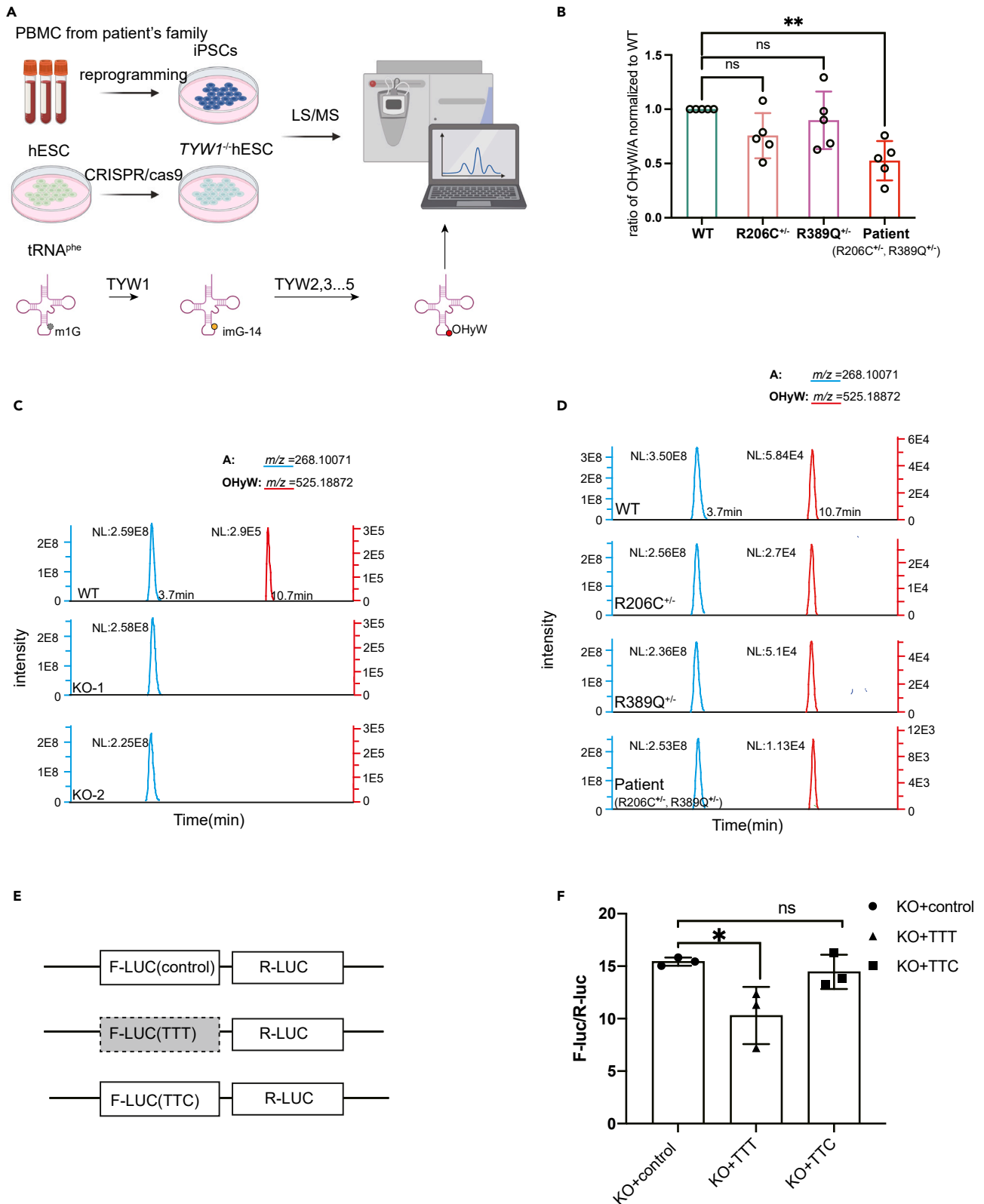
Figure 2. TYW1 mutation or depletion compromised OHyW formation and translation efficiency of UUU codon

(A) The upper panel shows the grouping and processing of the experiments. The lower panel shows the formation of OHyW of tRNA^{phe}.

(B) The ratio of OHyW/A in iPSCs of patient and his father (R206C$^{+/-}$) and mother (R389Q$^{+/-}$) compared to healthy control (WT). $n = 5$ independent replicates, data are presented as mean ± SD. **$p < 0.01$ from ordinary one-way ANOVA multiple comparisons.

(C) Mass spectral peaks of Adenosine (A) and Hydroxywybutosine (OHyW) from wild-type (WT) and TYW1-knockout (KO-1, KO-2) hESCs, respectively.

(D) Mass spectral peaks of Adenosine (A) and Hydroxywybutosine (OHyW) from healthy control, patient, patient's father, and mother, respectively.

(E) The schematic shows the constructs used in F.

(F) Luciferase reporter assay shows the ratio of F-luc/R-luc when cells transfected with different plasmids as shown in E. $n = 3$ independent replicates, data are presented as mean ± SD. *$p < 0.05$ from ordinary one-way ANOVA multiple comparisons.

In this study, we firstly proved that compound heterozygous variant compromised TYW1 protein half-life and OHyW level. The TYW1 knockout affects the translation efficiency of UUU codon. By establishing a TYW1-knockout human ES cell line, we found HERVK was elevated when TYW1 was depleted. Neuron differentiation was impaired in TYW1-knockout brain organoid, as well as in mouse models. The down-regulated UUU codon-rich protein, SMARCAD1, contributed to the elevated HERVK expression.

RESULTS

TYW1 variants lead to reduced protein stability without changing subcellular localization

Previously we have reported compound heterozygous variants, R206C and R389Q, of TYW1 contributed to cerebral palsy with severe intellectual disability.[7] In order to figure out if both variants affect protein stability, we expressed the mutated proteins in HEK293 cells and then synchronized the cells with cycloheximide and then determined the protein half-life. The cell viability was not significantly different between groups after cycloheximide treatment (data not shown); however, the mutated protein showed significantly reduced level 5 days after the cycloheximide treatment (Figures 1A and 1B), demonstrating reduced protein stability of both variant types. We also ask if TYW1 variants would change its subcellular localization. As reported by Takayuki et al., the catalysis of m1G37 to wybutosine derivatives of tRNA^{phe} occured at cytoplasm[25]; thus it is possible that TYW1 located in cytoplasm. We used DAPI and endoplasmic reticulum antibody to indicate nucleus and cytoplasm, respectively, as shown in Figure 1C; both wild-type (WT) and two variants of TYW1 showed clear localization in cytoplasm but not nucleus. Collectively, these results demonstrated that R206C and R389Q of TYW1 resulted in reduced protein stability, but the subcellular localization of TYW1 was not changed.

tRNA^{phe} hypomethylation compromised UUU codon translation in $TYW1^{-/-}$ human ESCs

TYW1 is a critical enzyme involved in OHyW modification in tRNA^{phe}[26]; thus we next explore if TYW1 variants would affect OHyW level. We previously generated patient-derived iPSCs (induced pluripotent stem cells).[27] iPSCs from healthy control and the patient's parents were also generated, but the data were not shown. TYW1-knockout hESCs were also generated by CRISPR-Cas9 (Figure S1A). Sanger sequencing demonstrated a 1 bp deletion and 1 bp insertion in two knockout clones, demonstrating frameshift in both clones (Figure S1B). Western blot further confirmed successful knockout of the protein as evidenced by depletion of the protein (Figure S1C). Morphologically, $TYW1^{-/-}$ hESCs look the same as WT hESCs and expressed the same level of main pluripotent markers (Figures S1D and S1E), indicating that self-renewal was not affected significantly by TYW1 depletion. Furthermore, the predicted off-target sites were examined and no off-target sites were found in either clone (Figure S2).

In order to evaluate how TYW1 variant or knockout affect the production of OHyW, we measured OHyW in patient-derived iPSCs and $TYW1^{-/-}$ hESCs by LS/MS (Figure 2A). We observed more than 50% drop of OHyW level in patient-derived cells (Figures 2B and 2D). By contrast, OHyW was completely undetectable in TYW1-knockout hESCs (Figure 2C). Collectively, these results demonstrated that TYW1 variant or depletion directly impeded the final formation of OHyW modification.

tRNA^{phe} decodes two kinds of codon, UUU and UUC. Previous study has indicated that tRNA^{phe} without wybutosine modification increased the frameshift events.[28] Interestingly, the 2′-o-methylation of tRNA^{phe} at Cm32 and Gm34 by FTSJ1 was reported to be prerequisite of G37 modification; thus FTSJ1 knockout affect the UUU decoding.[29] However, how TYW1 depletion may affect the decoding of UUU and UUC codons is not known. We applied the luciferase reporter system created by Li et al. to evaluate the translation efficiency of UUU codon in TYW1-knockout cells.[29] As shown in Figure 2E, the phenylalanine codon of Firefly luciferase was designed exclusively as either UUU or UUC; the WT Renilla luciferase served as internal control. As shown in Figure 2F, the relative activity of Firefly luciferase containing only UUU codon was significantly reduced compared to a WT Firefly luciferase, while the Firefly luciferase containing only UUC codon was not changed. We conclude that tRNA^{phe} hypomodification due to TYW1 knockout compromised UUU codon translation.

TYW1 depletion impaired neuron differentiation

Previously we have demonstrated that tRNA^{phe} hypomodification diminished neural proliferation[7]; however how tRNA^{phe} hypomodification may influence neural differentiation process is not known. Through Golgi staining we found that neurons from prefrontal cortex of Tyw1-knockout mice exhibit abnormal neuron morphology as manifested by significant reduced density of spine, as well as the length of dendritic spine (Figure 3A–3D). To give a deeper insight of how Tyw1 loss may lead to abnormal neuron morphology, we cultured primary neuron from $Tyw1^{-/-}$ E13.5 mice and observed that neuron differentiation from $Tyw1^{-/-}$ E13.5 mice exhibited less neurite length, as well as decreased number of segments (Figures 3E–3G), indicating impaired neural differentiation when Tyw1 was depleted.
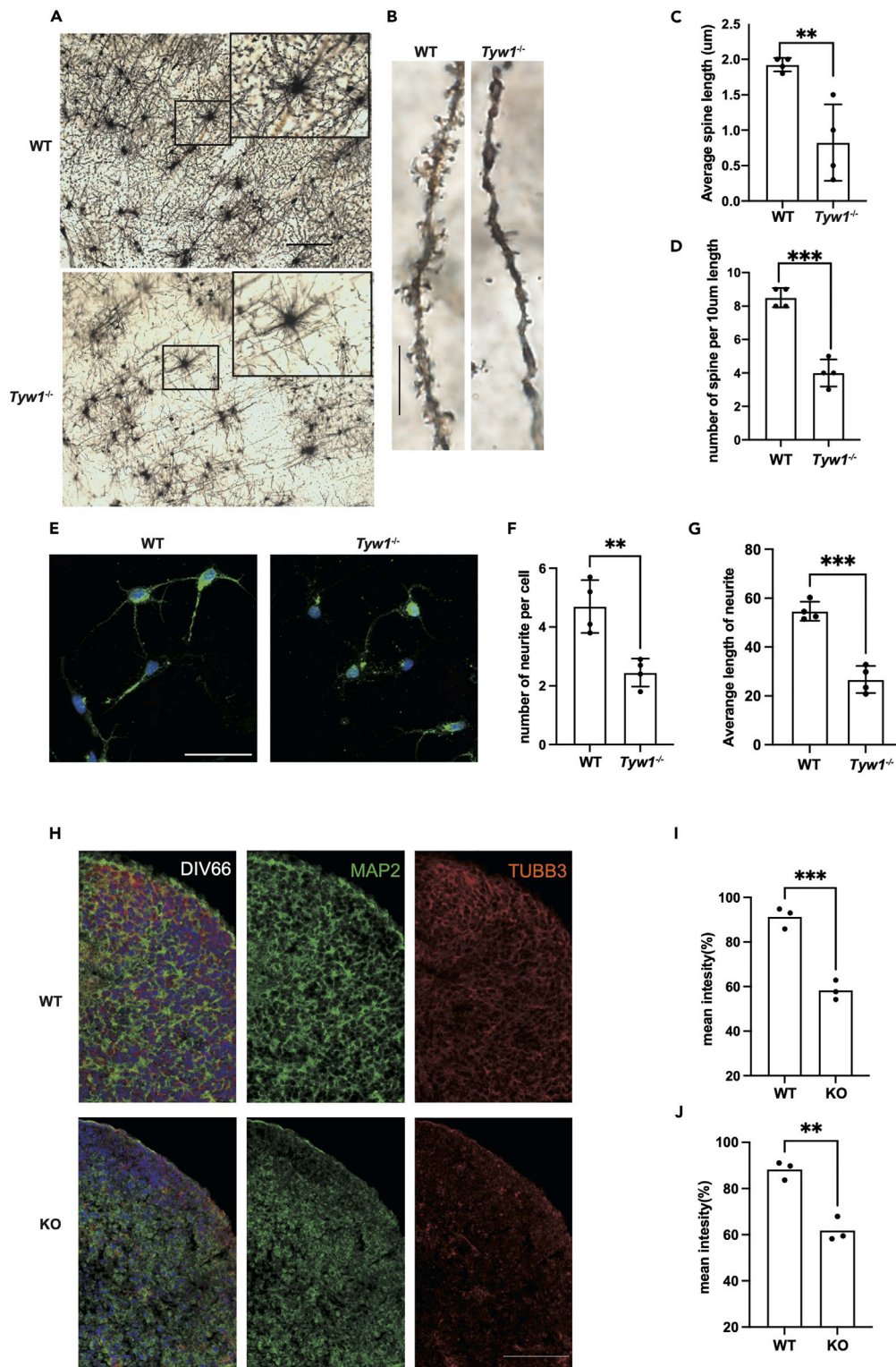
Figure 3. Neurons from *Tyw1*⁻/⁻ mouse and brain organoids show less complexity compared to control

(A) Golgi staining of adult brain from wild-type and *Tyw1*⁻/⁻ mice. Bar indicates 250 μm.

(B) Dendritic spines of wild-type and *Tyw1*⁻/⁻ mice as shown by Golgi staining. Bar indicates 5 μm.

Figure 3. *Continued*

(C and D) Bar plots show average spine length and number of spines of wild-type and *Tyw1*$^{-/-}$ mice. *n* = 4 independent replicates, data are presented as mean ± SD. **$p < 0.01$, ***$p < 0.001$ from unpaired t tests.

(E) Primary neuron culture of wild-type and *Tyw1*$^{-/-}$ mice for 10 days.

(F and G) Bar plots show average dendrite length and number of dendrites of primary neurons from wild-type and *Tyw1*$^{-/-}$ mice. *n* = 4 independent replicates, data are presented as mean ± SD. **$p < 0.01$, ***$p < 0.001$ from unpaired t tests.

(H) Immunostaining of WT and TYW1-knockout brain organoids (DIV 66) by MAP2 and β-Tubulin III. Bar indicates 100 μm.

(I and J) Bar plots show mean intensity of MAP2 and β-Tubulin III compared to WT. *n* = 3 independent replicates, data are presented as mean ± SD. **$p < 0.01$, ***$p < 0.001$ from unpaired t tests.

Brain organoids are good models to study different stages of human neural development.[30] Thus we differentiate *TYW1*$^{-/-}$ hESCs into brain organoids, and by 66 days *in vitro* (DIV) we observed significant lower intensity of neuronal markers of MAP2 and TUBB3 (Figures 3H–3J). These results showed clearly that neural differentiation was impaired when TYW1 was knocked out.

Elevated HERVK may contribute to impaired neuron differentiation in TYW1-knockout cell

In order to explore how TYW1 depletion may interfere neural differentiation process, we performed RNA sequencing (RNA-seq) analysis of *TYW1*$^{-/-}$ hESCs. We first performed GO enrichment analysis; the top terms of up-regulated genes are related to organ development process (Figure 4A). The top terms of down-regulated genes in *TYW1*$^{-/-}$ cells enriched in tRNA modification, suggesting tRNA modification was impaired in *TYW1*$^{-/-}$ cells (Figure 4B). Furthermore, we performed gene set enrichment analysis (GSEA) analysis, and the activated terms are related to neuron differentiation process, for example, the regulation of dendrite development and neuron genesis, suggesting neuron differentiation-related genes were dysregulated in *TYW1*$^{-/-}$ cells (Figure 4C). We also analyzed the expression of transposons in *TYW1*$^{-/-}$ cells. When we compared the proportions of up- and down-regulated repeat elements in each repeat family, we found HERVK was among the most dysregulated in *TYW1*$^{-/-}$ hESCs (Figure 4D). Although in general there were both up- and down-regulated locus of HERVK, the total expression of HERVK was up-regulated (Figure 4E). The up-regulated HERVK was further confirmed by quantitative reverse-transcription PCR (RT-qPCR) (Figure 4F). Previous study had reported that HERVK overexpression could induce NTRK3 overexpression and was detrimental to neuron differentiation.[17] Indeed, NTRK3 was also up-regulated in *TYW1*$^{-/-}$ hESCs (Figure 4F).

Next, we explore how HERVK may be up-regulated in *TYW1*$^{-/-}$ cells. It was previously reported that H3K9 methyltransferase SETDB1, recruiting other cofactors such as KAP1 and SMARCAD1, represses ERVs transcription by maintaining the heterochromatin state[31] (Figure 4G). In our case, neither SETDB1 nor KAP1 was changed globally in *TYW1*$^{-/-}$ cells. However, SMARCAD1 was significantly down-regulated (Figures 4H and 4I). Actually, according to the algorithms we developed previously,[7] SMARCAD1 was the most UUU-rich protein among the repression complex. The index of the predicted expression of each protein after TYW1 knockdown was indicated (Figure 4G).[7] Collectively, HERVK was de-repressed in *TYW1*$^{-/-}$ cells due to down-regulated SMARCAD1 and the elevated HERVK may have contributed to the impaired neuron differentiation.

SMARCAD1 overexpression improved the neuron differentiation in TYW1-knockout cell

To better elucidate the regulation of HERVK expression by SMARCAD1 and the regulation to neural differentiation, we generated doxycycline-inducible SMARCAD1-overexpressing hESCs in both WT and *TYW1*$^{-/-}$ cells and induced neural differentiation with brain organoids (Figure 5A). The effect of SMARCAD1 overexpression was validated at protein level (Figure 5B). Interestingly, we found the expression of HERVK was declined over time during brain organoids differentiation, while the expression of SMARCAD1 was increased, indicating the repression of HERVK by SMARCAD1 during neural differentiation (Figure 5C). As the expression of HERVK was predominantly in hESCs and neural induction stage, we speculated that HERVK exerted a regulation role at early stage of neuron differentiation. Moreover, the expression of HERVK was reduced by SMARCAD1 overexpression (Figure 5D), suggesting a direct regulation of HERVK expression by SMARCAD1. When we examined the neuronal marker expression, we found SMARCAD1 overexpression significantly improved the expression of MAP2 and TUBB3 in brain organoids (Figures 5E and 5F).

DISCUSSION

In this study, we showed both variants of TYW1 from patients exhibited significantly decreased protein stability compared to WT protein. Liquid chromatography-mass spectrometry (LC-MS) assays demonstrated that mutated TYW1 protein produced lower level of OHyW. Further luciferase reporter assay demonstrated that lack of tRNA^{phe} OHyW modification compromised translation with UUU codon in *TYW1*$^{-/-}$ hESCs. Neural differentiation was impaired in TYW1-knockout brain organoids, as well as in mouse models. Interestingly, we found HERVK was elevated in TYW1-knockout ES cells. The down-regulated SMARCAD1, one of the factors of the repression complex to repress the ERV, may explain the HERVK activation in *TYW1*$^{-/-}$ hESCs.

The G37 wybutosine modification of tRNA^{phe} (GAA), one of the most complex tRNA modification types, was conservative from archaea to eukaryotes species,[32,33] indicating its importance for translation accuracy. TYW1 catalyzes the tricyclic ring formation from m1G (37 position) of tRNA^{phe} to form 4-demethylwyosine (imG-14), which is crucial for the formation of OHyW in mammalian cells.[33] We have shown that TYW1 knockout completely diminished OHyW formation, while ∼50% level of OHyW can be detected from patient-derived cells. As we have shown
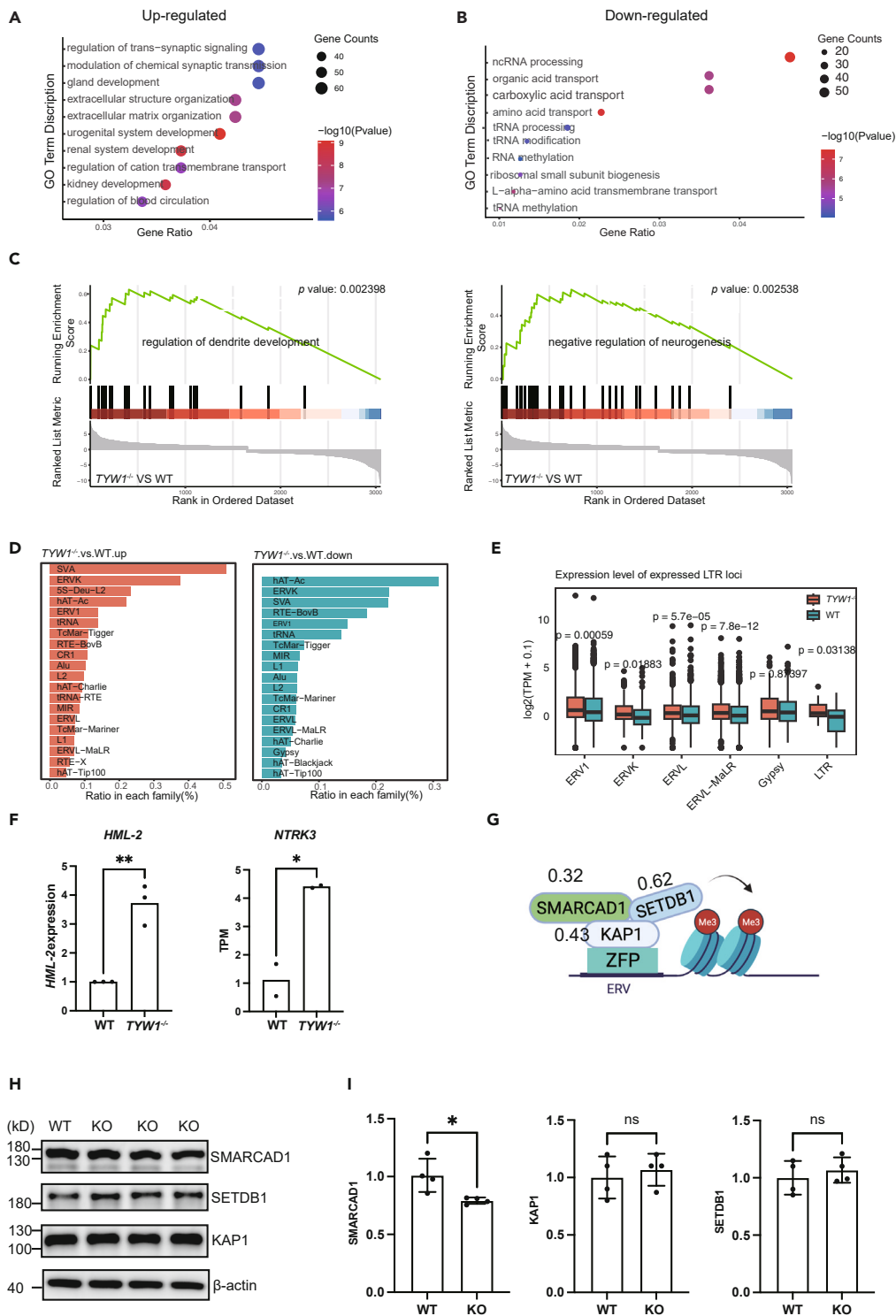
Figure 4. Transcriptional analysis of *TYW1*⁻/⁻ hESCs

(A and B) GO Enrichment analysis of up- and down-regulated genes in *TYW1*⁻/⁻ hESCs.

(C) GSEA results showed that the terms related to neuron differentiation was dysregulated in *TYW1*⁻/⁻ hESCs.

(D) Proportions of up (Left)- and down-regulated (Right) repeat elements in each repeat family in *TYW1*⁻/⁻ hESCs. The ratio was calculated as the locus number of up or down-regulated repeats divided by the total locus number of each repeat family.

(E) The expression of each family of LTR in *TYW1*⁻/⁻ and WT hESCs. *n* = 2 independent replicates, *p* value was calculated from unpaired t test.

Figure 4. Continued

(F) RT-qPCR shows the expression of HML2 in $TYW1^{-/-}$ and WT hESCs. n = 3 independent replicates, data are presented as mean ± SD. **p < 0.01, from unpaired t test. The expression of NTRK3 in $TYW1^{-/-}$ hESCs was calculated from RNA-seq, n=2 independent replicates, p value was calculated from unpaired t test.

(G) The schematic shows the repression complex of endogenous retrovirus. The ratio of each protein that may affect due to the tRNA^{phe} hypomodification was indicated individually.[7]

(H) Western blot analysis of the expression of the repression complex of endogenous retrovirus in $TYW1^{-/-}$ and WT hESCs.

(I) Mean intensity of SMARCAD1, SETDB1, KAP1 in $TYW1^{-/-}$ and WT hESCs. n = 4 independent replicates, data are presented as mean ± SD. *p < 0.05, from unpaired t test.

that the mutated protein exhibited less protein stability, we can conclude that the tRNA^{phe} from patient cells support lower level of OHyW formation due to reduced protein stability.

As we know, phenylalanine codon exists as two types, UUU and UUC. The G37 hyper-modification of tRNA^{phe} (GAA) is especially important to stabilize the codon and anticodon interaction when it comes with UUU codon. However, it is not known before how TYW1 may affect the translation of these codons. We have shown here that translation of UUU codon but not UUC codons was significantly impaired in TYW1-knockout cells, providing the direct evidence that protein enriched in UUU codon may subject to insufficient expression levels when TYW1 was depleted. Indeed, our previous study has demonstrated that key cell-cycle regulators were down-regulated in E13.5 mouse brain, contributing to a lower proliferation rate of neural progenitors.[7]

tRFs were reported to regulate LTR-retrotransposon transcription and silencing in mouse ES cells.[24] The mutation of some tRNA modification enzyme NSUN2 was reported to elicit increased expression of transposon element.[20] Thus, we were eager to explore if some retrotransposon was dis-regulated and affects the neural differentiation process in TYW1-knockout cells. We observed dis-regulation of transposon elements in $TYW1^{-/-}$ hESCs. Interestingly, HERVK was elevated in $TYW1^{-/-}$ hESCs. Cumulative studies have indicated that HERVK activation was detrimental to neural system. The activation of HERVK was reported to impair neuron differentiation.[17] Additionally, HERVK RNA could activate TLR8 and lead to neurodegenerative changes.[34] HERVK was repressed by ZNF417/587 in hESCs to avoid the induction of neurotoxic retroviral proteins and an interferon-like response during neuron differentiation.[18] Moreover, the expression of HERVK was reported to be elevated in some neurological disease, such as ALS, schizophrenia, and bipolar disorders.[35,36] Therefore, we speculate that the activated HERVK in $TYW1^{-/-}$ hESCs account for the impaired neuron differentiation.

The reason why HERVK was elevated in TYW1-knockout cells may be complex. We found that SMARCAD1 was down-regulated. As we have mentioned earlier, TYW1 knockout specially affects the decoding of UUU codon; SMARCAD1 was among the ERV repression complex of the most UUU-rich protein. Indeed, the expression of KAP1 and SETDB1 was not affected. Thus, the down-regulated SMARCAD1 may contribute to the overexpression of HERVK.

By exploring the expression profile of HERVK and SMARCAD1 during neuron differentiation process, we found that HERVK expression declined during neural differentiation, indicating that the detrimental effect of HERVK activation may dominant at early stage. Indeed, previous study showed that the HERVK activation at early stage but not later stage harmed neuron differentiation.[17] On contrary to the expression of HERVK, the expression of SMARCAD1 increased during the differentiation process, indicating the direct regulation of HERVK by SMARCAD1. The repression of HERVK by SMARCAD1 overexpression further supports this.

Taken together, our study demonstrated that loss of TYW1 affect the expression of UUU codon-enriched proteins. The incompetence of SMARCAD1/KAP1/SETDB1 repression complex contributed to elevated HERVK and thus impaired neuron differentiation. Our study provides a novel mechanism of how defect in TYW1 may regulate neuron differentiation through retrotransposon, enriching our understanding of how genetic lesions contribute to the neurodevelopmental disorders.

Limitations of the study

Our study demonstrated that HERVK activation due to insufficient SMARCAD1 expression contributed to impaired neuron differentiation when TYW1 was knocked out. In line with previous study,[17] the HERVK activation within neural induction stage is particularly harmful. The activation of neuron differentiation genes such as NTRK3 may explain how HERVK activation within neural induction stage may affect later neuron differentiation; however future studies are needed to clarify this in detail.

STAR★METHODS

Detailed methods are provided in the online version of this paper and include the following:

- KEY RESOURCES TABLE
- RESOURCE AVAILABILITY
  - Lead contact
  - Materials availability
  - Data and code availability
- EXPERIMENTAL MODEL AND STUDY PARTICIPANT DETAILS
  - Animals
  - Cell lines
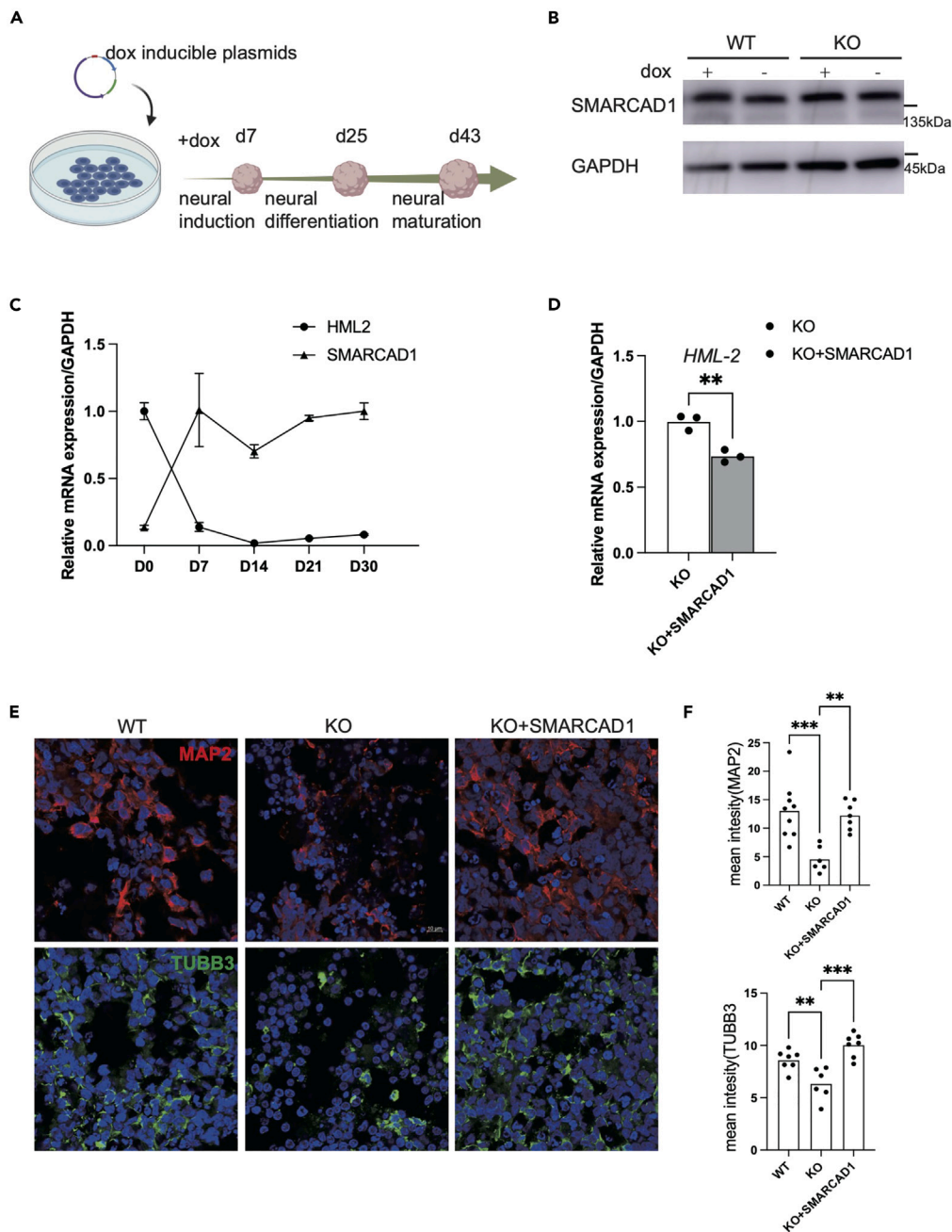
Figure 5. SMARCAD1 overexpression improved the neuron differentiation in TYW1-knockout cell

(A) Schematic showing the strategy of examine the effect of SMARCAD1 overexpression during neural development.

(B) Representative image of western blot to detect the expression of SMARCAD1 in WT and TYW1$^{-/-}$ cells with or without SMARCAD1 overexpression.

(C) RT-qPCR to determine the mRNA expression of HERVK and SMARCAD1 during the brain organoids differentiation process. Data are presented as mean ± SD.

(D) RT-qPCR to determine the mRNA expression of HERVK in TYW1$^{-/-}$ hESC with or without SMARCAD1 overexpression. Data are presented as mean ± SD. **$p < 0.01$, from unpaired t test.

(E) Immunostaining of brain organoids (DIV 35) by MAP2 and β-Tubulin III. Bar indicates 10 μm.

(F) Bar plots show mean intensity of MAP2 and β-Tubulin III of WT, KO and KO + SMARCAD1 organoids. 6–9 organoids from each group were used, data are presented as mean ± SD. **$p < 0.01$, ***$p < 0.001$ from ordinary one-way ANOVA multiple comparisons.

- METHOD DETAILS
  - Determination of TYW1 protein half-life
  - Determination of TYW1 subcellular localization
  - Generation of TYW1 knockout hESCs by CRISPR
  - Generation of SMARCAD1 expressing hESCs
  - Mass spectrometry
  - Western blot analysis
  - RT-qPCR
  - Immunofluorescence
  - Dual luciferase assay
  - Culture of primary neurons
  - Golgi staining
  - Generation of cerebral organoids from hESCs
  - RNA-seq
- QUANTIFICATION AND STATISTICAL ANALYSIS

SUPPLEMENTAL INFORMATION

Supplemental information can be found online at https://doi.org/10.1016/j.isci.2024.109748.

AUTHOR CONTRIBUTIONS

Conceptualization, C.S. and H.H.; methodology, R.G. and C.S.; writing – original draft, C.S. and R.G.; writing – review and editing, N.L., H.H., D.Z., Y.S., K.X., and D.H.; funding acquisition, C.S., H.H., and Y.S.; supervision, C.S., H.H., and N.L.

DECLARATION OF INTERESTS

The authors declare no competing interests.

REFERENCES

1. Orellana, E.A., Siegal, E., and Gregory, R.I. (2022). tRNA dysregulation and disease. Nat. Rev. Genet. 23, 651–664. https://doi.org/10.1038/s41576-022-00501-9.

2. Blanco, S., Dietmann, S., Flores, J.V., Hussain, S., Kutter, C., Humphreys, P., Lukk, M., Lombard, P., Treps, L., Popis, M., et al. (2014). Aberrant methylation of tRNAs links cellular stress to neuro-developmental disorders. EMBO J. 33, 2020–2039. https://doi.org/10.15252/embj.201489282.

3. Nagayoshi, Y., Chujo, T., Hirata, S., Nakatsuka, H., Chen, C.W., Takakura, M., Miyauchi, K., Ikeuchi, Y., Carlyle, B.C., Kitchen, R.R., et al. (2021). Loss of Ftsj1 perturbs codon-specific translation efficiency in the brain and is associated with X-linked intellectual disability. Sci. Adv. 7, eabf3072. https://doi.org/10.1126/sciadv.abf3072.

4. Braun, D.A., Rao, J., Mollet, G., Schapiro, D., Daugeron, M.C., Tan, W., Gribouval, O., Boyer, O., Revy, P., Jobst-Schwan, T., et al. (2017). Mutations in KEOPS-complex genes cause nephrotic syndrome with primary microcephaly. Nat. Genet. 49, 1529–1538. https://doi.org/10.1038/ng.3933.

5. Suzuki, T. (2021). The expanding world of tRNA modifications and their disease relevance. Nat. Rev. Mol. Cell Biol. 22, 375–392. https://doi.org/10.1038/s41580-021-00342-0.

6. Jenner, L.B., Demeshkina, N., Yusupova, G., and Yusupov, M. (2010). Structural aspects of messenger RNA reading frame maintenance by the ribosome. Nat. Struct. Mol. Biol. 17, 555–560. https://doi.org/10.1038/nsmb.1790.

7. Li, N., Zhou, P., Tang, H., He, L., Fang, X., Zhao, J., Wang, X., Qi, Y., Sun, C., Lin, Y., et al. (2022). In-depth analysis reveals complex molecular aetiology in a cohort of idiopathic cerebral palsy. Brain 145, 119–141. https://doi.org/10.1093/brain/awab209.

8. Suzuki, Y., Noma, A., Suzuki, T., Senda, M., Senda, T., Ishitani, R., and Nureki, O. (2007). Crystal structure of the radical SAM enzyme catalyzing tricyclic modified base formation in tRNA. J. Mol. Biol. 372, 1204–1214. https://doi.org/10.1016/j.jmb.2007.07.024.

9. Harnett, D., Ambrozkiewicz, M.C., Zinnall, U., Rusanova, A., Borisova, E., Drescher, A.N., Couce-Iglesias, M., Villamil, G., Dannenberg, R., Imami, K., et al. (2022). A critical period of translational control during brain development at codon resolution. Nat. Struct. Mol. Biol. 29, 1277–1290. https://doi.org/10.1038/s41594-022-00882-9.

10. Hirabayashi, Y., and Gotoh, Y. (2010). Epigenetic control of neural precursor cell fate during development. Nat. Rev. Neurosci. 11, 377–388. https://doi.org/10.1038/nrn2810.

11. Bian, S., and Sun, T. (2011). Functions of noncoding RNAs in neural development and neurological diseases. Mol. Neurobiol. 44, 359–373. https://doi.org/10.1007/s12035-011-8211-3.

12. Choi, J., Lyons, D.B., Kim, M.Y., Moore, J.D., and Zilberman, D. (2020). DNA Methylation

and Histone H1 Jointly Repress Transposable Elements and Aberrant Intragenic Transcripts. Mol. Cell 77, 310–323.e7. https://doi.org/10.1016/j.molcel.2019.10.011.

13. Cui, X., Jin, P., Cui, X., Gu, L., Lu, Z., Xue, Y., Wei, L., Qi, J., Song, X., Luo, M., et al. (2013). Control of transposon activity by a histone H3K4 demethylase in rice. Proc. Natl. Acad. Sci. USA 110, 1953–1958. https://doi.org/10.1073/pnas.1217020110.

14. Pontis, J., Pulver, C., Playfoot, C.J., Planet, E., Grun, D., Offner, S., Duc, J., Manfrin, A., Lutolf, M.P., and Trono, D. (2022). Primate-specific transposable elements shape transcriptional networks during human development. Nat. Commun. 13, 7178. https://doi.org/10.1038/s41467-022-34800-w.

15. Jönsson, M.E., Garza, R., Sharma, Y., Petri, R., Söderstem, E., Johansson, J.G., Johansson, P.A., Atacho, D.A., Pircs, K., Madsen, S., et al. (2021). Activation of endogenous retroviruses during brain development causes an inflammatory response. EMBO J. 40, e106423. https://doi.org/10.15252/embj.2020106423.

16. Patoori, S., Barnada, S.M., Large, C., Murray, J.I., and Trizzino, M. (2022). Young transposable elements rewired gene regulatory networks in human and chimpanzee hippocampal intermediate progenitors. Development 149, dev200413. https://doi.org/10.1242/dev.200413.

17. Padmanabhan Nair, V., Liu, H., Ciceri, G., Jungverdorben, J., Frishman, G., Tchieu, J., Cederquist, G.Y., Rothenaigner, I., Schorpp, K., Klepper, L., et al. (2021). Activation of HERV-K(HML-2) disrupts cortical patterning and neuronal differentiation by increasing NTRK3. Cell Stem Cell 28, 1566–1581.e8. https://doi.org/10.1016/j.stem.2021.04.009.

18. Turelli, P., Playfoot, C., Grun, D., Raclot, C., Pontis, J., Coudray, A., Thorball, C., Duc, J., Pankevich, E.V., Deplancke, B., et al. (2020). Primate-restricted KRAB zinc finger proteins and target retrotransposons control gene expression in human neurons. Sci. Adv. 6, eaba3200. https://doi.org/10.1126/sciadv.aba3200.

19. Sharma, U., Conine, C.C., Shea, J.M., Boskovic, A., Derr, A.G., Bing, X.Y., Belleannee, C., Kucukural, A., Serra, R.W., Sun, F., et al. (2016). Biogenesis and function of tRNA fragments during sperm maturation and fertilization in mammals. Science 351, 391–396. https://doi.org/10.1126/science.aad6780.

20. Genenncher, B., Durdevic, Z., Hanna, K., Zinkl, D., Mobin, M.B., Senturk, N., Da Silva, B., Legrand, C., Carré, C., Lyko, F., and Schaefer, M. (2018). Mutations in Cytosine-5 tRNA Methyltransferases Impact Mobile Element Expression and Genome Stability at Specific DNA Repeats. Cell Rep. 22, 1861–

1874. https://doi.org/10.1016/j.celrep.2018.01.061.

21. Chou, H.J., Donnard, E., Gustafsson, H.T., Garber, M., and Rando, O.J. (2017). Transcriptome-wide Analysis of Roles for tRNA Modifications in Translational Regulation. Mol. Cell 68, 978–992.e4. https://doi.org/10.1016/j.molcel.2017.11.002.

22. Marquet, R., Isel, C., Ehresmann, C., and Ehresmann, B. (1995). tRNAs as primer of reverse transcriptases. Biochimie 77, 113–124. https://doi.org/10.1016/0300-9084(96)88114-4.

23. Saigo, K. (1986). Unusual clustering of the genes for primer tRNAs for reverse transcription of retrotransposons in Drosophila. Nucleic Acids Res. 14, 9526. https://doi.org/10.1093/nar/14.23.9526.

24. Schorn, A.J., Gutbrod, M.J., LeBlanc, C., and Martienssen, R. (2017). LTR-Retrotransposon Control by tRNA-Derived Small RNAs. Cell 170, 61–71.e11. https://doi.org/10.1016/j.cell.2017.06.013.

25. Ohira, T., and Suzuki, T. (2011). Retrograde nuclear import of tRNA precursors is required for modified base biogenesis in yeast. Proc. Natl. Acad. Sci. USA 108, 10502–10507. https://doi.org/10.1073/pnas.1105645108.

26. Young, A.P., and Bandarian, V. (2018). TYW1: A Radical SAM Enzyme Involved in the Biosynthesis of Wybutosine Bases. Methods Enzymol. 606, 119–153. https://doi.org/10.1016/bs.mie.2018.04.024.

27. Sun, C., Zhou, P., Yuan, S., Guo, R., Zhang, Z., Xu, Q., Han, D., He, L., Tang, H., Xu, K., et al. (2020). Generation of an induced pluripotent stem cell line SYSUi-004-A from a child of microcephaly with TYW1 mutations. Stem Cell Res. 45, 101783. https://doi.org/10.1016/j.scr.2020.101783.

28. Carlson, B.A., Kwon, S.Y., Chamorro, M., Oroszlan, S., Hatfield, D.L., and Lee, B.J. (1999). Transfer RNA modification status influences retroviral ribosomal frameshifting. Virology 255, 2–8. https://doi.org/10.1006/viro.1998.9569.

29. Li, J., Wang, Y.N., Xu, B.S., Liu, Y.P., Zhou, M., Long, T., Li, H., Dong, H., Nie, Y., Chen, P.R., et al. (2020). Intellectual disability-associated gene ftsj1 is responsible for 2'-O-methylation of specific tRNAs. EMBO Rep. 21, e50095. https://doi.org/10.15252/embr.202050095.

30. Giandomenico, S.L., Sutcliffe, M., and Lancaster, M.A. (2021). Generation and long-term culture of advanced cerebral organoids for studying later stages of neural development. Nat. Protoc. 16, 579–602. https://doi.org/10.1038/s41596-020-00433-w.

31. Sachs, P., Ding, D., Bergmaier, P., Lamp, B., Schlagheck, C., Finkernagel, F., Nist, A., Stiewe, T., and Mermoud, J.E. (2019). SMARCAD1 ATPase activity is required to silence endogenous retroviruses in embryonic stem cells. Nat. Commun. 10,

1335. https://doi.org/10.1038/s41467-019-09078-0.

32. de Crecy-Lagard, V., Brochier-Armanet, C., Urbonavicius, J., Fernandez, B., Phillips, G., Lyons, B., Noma, A., Alvarez, S., Droogmans, L., Armengaud, J., and Grosjean, H. (2010). Biosynthesis of wyosine derivatives in tRNA: an ancient and highly diverse pathway in Archaea. Mol. Biol. Evol. 27, 2062–2077. https://doi.org/10.1093/molbev/msq096.

33. Noma, A., Kirino, Y., Ikeuchi, Y., and Suzuki, T. (2006). Biosynthesis of wybutosine, a hyper-modified nucleoside in eukaryotic phenylalanine tRNA. EMBO J. 25, 2142–2154. https://doi.org/10.1038/sj.emboj.7601105.

34. Dembny, P., Newman, A.G., Singh, M., Hinz, M., Szczepek, M., Krüger, C., Adalbert, R., Dzaye, O., Trimbuch, T., Wallach, T., et al. (2020). Human endogenous retrovirus HERV-K(HML-2) RNA causes neurodegeneration through Toll-like receptors. JCI Insight 5, e131093. https://doi.org/10.1172/jci.insight.131093.

35. Simula, E.R., Arru, G., Zarbo, I.R., Solla, P., and Sechi, L.A. (2021). TDP-43 and HERV-K Envelope-Specific Immunogenic Epitopes Are Recognized in ALS Patients. Viruses 13, 2301. https://doi.org/10.3390/v13112301.

36. Arru, G., Galleri, G., Deiana, G.A., Zarbo, I.R., Sechi, E., Bo, M., Cadoni, M.P.L., Corda, D.G., Frau, C., Simula, E.R., et al. (2021). HERV-K Modulates the Immune Response in ALS Patients. Microorganisms 9, 1784. https://doi.org/10.3390/microorganisms9081784.

37. Schindelin, J., Arganda-Carreras, I., Frise, E., Kaynig, V., Longair, M., Pietzsch, T., Preibisch, S., Rueden, C., Saalfeld, S., Schmid, B., et al. (2012). Fiji: an open-source platform for biological-image. analysis. Nat. Methods 9, 676–682. https://doi.org/10.1038/nmeth.2019.

38. Liao, Y., Smyth, G.K., and Shi, W. (2014). featureCounts: an efficient general purpose program for assigning sequence reads to genomic features. Bioinformatics 30, 923–930. https://doi.org/10.1093/bioinformatics/btt656.

39. Love, M.I., Huber, W., and Anders, S. (2014). Moderated estimation of fold change and dispersion for RNA-seq data with DESeq2. Genome Biol. 15, 550. https://doi.org/10.1186/s13059-014-0550-8.

40. Dobin, A., Davis, C.A., Schlesinger, F., Drenkow, J., Zaleski, C., Jha, S., Batut, P., Chaisson, M., and Gingeras, T.R. (2013). STAR: ultrafast universal RNA-seq aligner. Bioinformatics 29, 15–21. https://doi.org/10.1093/bioinformatics/bts635.

41. Robinson, M.D., McCarthy, D.J., and Smyth, G.K. (2010). edgeR: a Bioconductor. package for differential expression analysis of digital gene expression data. Bioinformatics 26, 139–140. https://doi.org/10.1093/bioinformatics/btp616.

STAR★METHODS

KEY RESOURCES TABLE

REAGENT or RESOURCE	SOURCE	IDENTIFIER
Antibodies		
Anti-HA	CST	Cat#3724S; RRID:AB_1549585
Anti-ER	Novus Biologicals	Cat#nbp-2-75482
Anti-GFP	Santa Cruz	Cat#sc-9996; RRID: AB_627695
Anti-MAP2	Abcam	Cat#ab183830; RRID : AB_2895301
Anti-TUBB3	Abcam	Cat#ab78078; RRID: AB_2256751
Anti-MAP2	Proteintech	Cat#17490-1-AP; RRID:AB_2137880
Anti-TUBB3	Sigma-Aldrich	Cat#MAB1637; RRID: AB_2210524
Anti-SMARCAD1	Boster	Cat#A06049-1
Anti-SOX2	Applied Stemcell	Cat#ASA-0120; RRID:AB_2827681
Anti-Tra-1-81	Applied Stemcell	Cat#ASA-0170
Anti-NANOG	R&D	Cat#AF1997; RRID: AB_355097
Anti-OCT4	Abcam	Cat#ab181557, RRID: AB_2687916
Anti-SETDB1	Novus Biologicals	Cat#nbp-2-20321
Anti-TYW1	customized	N/A
Anti-GAPDH	Boster	Cat#BM1623; RRID:AB_2885058
Anti-ACTB	Beyotime	Cat#AF0003; RRID:AB_2893353
Anti-KAP1	CST	Cat#4142s; RRID: AB_2209886
HRP Conjugated Anti-Mouse	Beyotime	Cat#A0216; RRID:AB_2860575
HRP Conjugated Anti-Rabbit	Beyotime	Cat#A0208; RRID:AB_2892644
Bacterial and virus strains		
Dh5-α	TSINGKE	TSC-C01-10
Chemicals, peptides, and recombinant proteins		
DAPI	CST	8961S
Matrigel	Corning	354277
Y-27632	selleck	S1049
Puromycin	InvivoGen	58-58-2
benzonase	novoprotein	M046-01A
PDE1	Sigma-Aldrich	P3243
bacterial alkaline phosphatase	Takara	2120A
poly-D-lysine	Sigma-Aldrich	P6407
B27	Thermo Fisher Scientific	12587010
Glutamax	Thermo Fisher	35050061
Doxycycline	Sigma-Aldrich	D3072
Dorsomorphin	selleck	S7840
SB-431542	selleck	S1067
E6 medium	Thermo Fisher	A1516401
Neural basal A medium	Thermo Fisher	21103049
EGF	PeproTech	AF-100-15
FGF2	PeproTech	100-18B
BDNF	PeproTech	450-02-50

Continued

REAGENT or RESOURCE	SOURCE	IDENTIFIER
NT-3	PeproTech	450-03-10
XAV-939	Tocris	3748
cycloheximide	Sigma-Aldrich	239765
PGM1 medium	cellapy	CA1007500
Critical commercial assays		
Dual-Luciferase Assay	Promega	E1910
LipofectamineTM 3000 Reagent	Thermo Fisher	L3000005
miRcute miRNA isolation kit	Tiangen	DP501
Rapid GolgiStain Kit	FD Neurotech	PK401
color reverse transcription kit	EZBioscience	A0010CGQ
SYBR green qPCR Mix	EZBioscience	CQ20
NeonTM Transfection System 100 mL Kit	Thermo Fisher	MPK10096
Deposited data		
Raw and analyzed data	This study	GSE262470
Experimental models: Cell lines		
hESC (the H1 line)	Wicell	N/A
HEK293 cells	ATCC	N/A
Human iPSC healthy control	This study	N/A
Human iPSC patient	This study	N/A
Human iPSC patient's father	This study	N/A
Human iPSC patient's mother	This study	N/A
Experimental models: Organisms/strains		
Mouse: C57BL/6J	Mice bred in-house	N/A
Oligonucleotides		
SgRNA for TYW1: GCATCGTGTGATGAGTCGAG GGG	This study	N/A
Primers for RT-PCR and genomic PCR, see Table S1	This study	N/A
Recombinant DNA		
pBI-CMV2-TYW1-WT	This study	N/A
pBI-CMV2-TYW1-R206C	This study	N/A
pBI-CMV2-TYW1-R389Q	This study	N/A
Px459-sgTYW1	This study	N/A
PB-TetON-MiniCMV- Smarcad1- PGK-puro-T2A-rtTA	This study	N/A
pmirGlo vectors	Li et al.[29]	N/A
Software and algorithms		
Fiji(ImageJ)	Schindelin et al.[37]	https://imagej.net/software/fiji/
Prism 9.0	Graphpad	https://www.graphpad.com
featureCounts (v2.0.0)	Liao et al.[38]	http://subread.sourceforge.net/
DESeq2 (v1.28.1)	Love et al.[39]	https://bioconductor.org/packages/release/bioc/html/DESeq2.html
STAR (v2.7.4a)	Dobin et al.[40]	https://github.com/alexdobin/STAR
edgeR (v3.34.1)	Robinson et al.[41]	https://bioconductor.org/packages/release/bioc/html/edgeR.html

RESOURCE AVAILABILITY

Lead contact

Further information and requests for resources and reagents should be directed to and will be fulfilled by the lead contact, Hao Hu (huh@cougarlab.org).

Materials availability

This study did not generate new unique reagents.

Data and code availability

- The raw data of bulk RNA-seq have been deposited in NCBI's GeneExpression Omnibus (GEO) with the accession number GEO: GSE262470. All datasets reported in this work are available from the lead contact upon request.
- This paper does not report original code.
- Any additional information required to reanalyze the data reported in this paper is available from the lead contact upon request.

EXPERIMENTAL MODEL AND STUDY PARTICIPANT DETAILS

Animals

All mice experiments in this work were approved by the institutional animal care and use committee in the Guangzhou Medical University (registration No. 2019-436, 2019-694). In this study, all mice, either wild-type or mutant, were generated from the C57BL/6J strain and provided by the Cyagen Biosciences (Guangzhou, China). Mice were housed in a temperature-controlled room at 20°C–24°C. For animal experiments, Tyw1 knockout male and female mice (sex balance) at age of 6–8 weeks were used. Embryos at embryonic day 13.5 (E13.5) were used for primary neuron cultures.

Cell lines

H1 hESCs (male) and iPSCs(healthy control is a female, patient's iPSC is male, patient's father's iPSC is male, patient's mother's iPSC is female) were maintained in PGM1 medium (CA1007500,cellapy) on Matrigel (354277,Corning)coated plates at 37°C in hypoxic incubator. The medium was changed daily. HeLa (female) and HEK293T cells(female) were cultured in DMEM medium containing 10% FBS at 37°C with 5% CO_2.

METHOD DETAILS

Determination of TYW1 protein half-life

HEK293T cells were grown in DMEM medium supplemented with 10% FBS at 37°C with 5% CO_2. Transfection was performed when cells reach 70% confluence with Lipofectamine 3000 Reagent (L3000150,ThermoFisher Scientific). Plasmids pBI-CMV2 expressed either wild-type or mutated TYW1 with HA tag were used. The cells were treated with 20 μg/mL cycloheximide 48 h after transfection and cells were collected at 0 h, 24h, 48h, 96h, 120h after cycloheximide treatment. The cell lysates were subjected to western blot to determine the TYW1 protein content and GFP serves as internal reference. Western blotting was performed to semi-quantify the expression of HA- TYW1 protein with GFP protein as the internal reference. The antibodies used are anti-HA-tag (3724S, Cell Signaling Technology, USA) and anti-GFP (B-2, sc-9996, Santa Cruz Biotechnology, USA) antibodies.

Determination of TYW1 subcellular localization

HeLa cells were cultured in DMEM medium containing 10% FBS at 37°C with 5% CO_2. The cells were transfected with plasmids as indicated in protein half-life experiments. 24 h after transfection, the cells were fixed and incubated with anti-HA-tag or anti-ER antibody and imaged. The colocalization of HA-TYW1 with DAPI or ER was analyzed with colocalization finder tool from Fiji software. Pearson's_R > 0.5 was defined as colocalization.

Generation of TYW1 knockout hESCs by CRISPR

H1 hESCs were treated with 10uM Y-27632 (S1049, selleck) for 12 h when growing to 70% confluence before transfection. 10^6 cells were transfected with 2ug px459 plasmid expressing cas9 and sgRNA targeting TYW1 using Neon Transfection system. The transfected cells were seeded at low density in a six well plate. Puromycin was used from 0.1 to 0.3 μg/mL for different wells in order to get single cell clones. Single-cell clones were picked for further expansion and genomic PCR.

Generation of SMARCAD1 expressing hESCs

To generate doxycycline inducible SMARCAD1 expressing hESCs, we first clone human SMARCAD1 coding sequence into a piggyBac vector with tet inducible promoter and puromycin resistance gene. The hESCs was treated with 10uM Y-27632 before neon electroporation. 2ug doxycycline inducible SMARCAD1 and 200ng piggyBac transposase was transfected into hESCs together. 48 h after transfection, puromycin was added at 0.4ug/mL for 5 days. Doxycycline was added at 1ug/mL to induce the expression of SMARCAD1.

Mass spectrometry

The small RNA fraction was extracted using miRcute miRNA isolation kit (DP501,Tiangen).The same amount of miRNAs (~4ug) was hydrolyzed with 0.5ul benzonase, 5ul PDE1 and 0.5ul bacterial alkaline phosphatase at 37°C for 3h. After complete hydrolysis, the solution was loaded onto Amicon Ultra-0.5 filter (Merck Millipore) to remove the nuclease and concentrated to ≤300 μL by repeated centrifugation according to the manual. The concentrate was collected and freeze-dried. The nucleosides were dissolved and separated on a C18 column(186002352, Waters). The peaks of specific nucleosides were recognized by their M + H weight: 268.10345(A), 284.09895(G), 244.09222 (C), 245.07635(U), and 525.19397 (OHyW). The ratio of OHyW to the sum of A was determined based on the calculated concentrations.

Western blot analysis

The brain tissue or cells were lysed with RIPA buffer containing protease inhibitor cocktail. The protein lysates were separated by sodium dodecyl sulfate-polyacrylamide gel electrophoresis (SDS-PAGE), and then the proteins were transferred to 0.2 μm PVDF membranes. After blocking with 5% (w/v) non-fat dried milk, the membranes were incubated with the corresponding primary antibodies overnight at 4°C. Membranes were then washed three times with TBST and incubated with HRP-conjugated secondary antibody at room temperature for 60 min. After washing three times with TBST, the membranes were treated with the chemiluminescent substrates (EpiZyme), and imaging was performed using the Amersham Imager 680 (GE Healthcare). The primary antibodies used are as following: anti-TYW1(customized), anti-SMARCAD1(A06049-1,boster), anti-KAP1(4124s, CST),SETDB1(nbp-2-20321,Novus).

RT-qPCR

Total RNA was extracted using RNA purification kit (EZBioscience) and 1ug RNA was used to synthesize cDNA using the color reverse transcription kit (EZBioscience). 10 ng cDNA was used for quantitative RT–PCR (qRT–PCR) reaction using the SYBR green qPCR Mix (EZBioscience) on the LightCycle 480II (Roche). The relative expression of genes was calculated using ΔΔCT method. The primers used in this study are listed in Table S1.

Immunofluorescence

Cells were fixed with 4% (v/v) paraformaldehyde for 20 min, washed with PBS, blocked using 0.3% (v/v) Triton X-100 in PBS with 1% (w/v) BSA for 1 h. For immunocytochemistry, cells were incubated with primary antibodies diluted in the same blocking buffer at 4°C overnight. Following three washes, cells were incubated with appropriate AlexaFluor secondary antibodies (1:500; Molecular Probes) and DAPI (1:1000; Thermo Fisher) diluted in the blocking buffer for 1 h at room temperature. After washing, cells were taken images by the Nikon Eclipse Ni-E. The antibodies used including: anti-OCT4(ab181557), anti-SOX2(ASA-0120), anti-NANOG(AF1997), anti-tra-1-81(ASA-0170), anti-HA tag(3724S, CST).The brain organoids were fixed with 4% (v/v) paraformaldehyde for 30 min and dehydrated with 30% sucrose and then embedded with OCT, snap frozen and sectioned to 10um sections. The sections were immune-stained and imaged with the same method as above. The antibodies used including: anti-MAP2(ab183830), anti-beta III tubulin (MAB1637).

Dual luciferase assay

We used phenylalanine codon edited luciferase reporter plasmids as reported by Li et al.[29] 40 ng of reporter plasmids (pmirGlo empty vector or pmirGlo mutated vector) was transfected into WT hESCs and *TYW1* knockout cells in a 24-well plate using Lipofectamine 3000. After 24 h, the cells in the 24-well plate were treated according to the manual of Dual-Glo Luciferase Assay kit (Promega, E1910).The translation efficiency of the reporter was indicated by F-luc activity normalized by R-luc.

Culture of primary neurons

E13.5 mouse embryo brains were taken out from *Tyw1*^{+/−} pregnant dam. Cortex in each brain was dissected separately and collected in Hibernate-E supplemented with 2% B27 on ice. Single cells were obtained by using 0.05% trypsin (containing 0.2 mM EDTA) digestion for 10 min at 37°C. After filtration with 70 μm strainer and centrifugation, cells were seeded in DMEM/F12 medium containing 10%FBS in poly-D-lysine coated plates. After about 4 h, the medium was changed with Neurobasal medium containing 2% B27 Plus Supplement, 0.25% Glutamax and 25 μM glutamate. After three days, glutamate was removed from the medium.

Golgi staining

Brain tissue was fixed according to the FD rapid Golgistain kit. Briefly, tissue was immersed in a mixture of solution A and B in dark for 2 weeks and then transferred to solution C in dark for 72 h. Then the tissue was embedded and sliced into 100 μm sections. The slices were washed with ddH2O twice, then immersed in a mixture of 25% solution D and 25% solution E for 10 min and then washed with ddH$_2$O twice. For dehydration of sections, slides were placed in 50%, 75% and 90% ethanol for 5 min, followed by rinsing with 100% ethanol 4 times. After that, sections were transferred into ammonia solution (3:1 ammonia to ddH$_2$O) for 6 min. In the final step, slides were cleared by xylene and mounted by Entellan glue. Sections were kept in the dark until imaging. The images were taken by confocal microscope.

Generation of cerebral organoids from hESCs

The hESCs colonies were dissociated into single cells using Accutase. On day 0, a total of 9000 cells were plated into each well of an ultra-low-attachment 96-well plate (Corning) for single EB formation. The EB formation medium consisted of PGM1 medium with the ROCK inhibitor Y-27632 to a final concentration of 10 μM. On day 1, for neural induction and differentiation, E6 medium supplemented with 2.5 μM Dorsomorphin (DM) and 10 μM SB-431542 (SB) was used. Optionally, 2.5 μM XAV-939 (XAV) can be added for the first five days. Media changes are performed every other day. On day 6, E6 medium containing DM and SB is replaced with neural basal A medium (10888022, Thermo Fisher Scientific) supplemented with EGF (20 ng/mL) and FGF2 (20 ng/mL) for the 19 days with daily medium change in the first 10 days, and every other day medium changes for the subsequent 9 days. To promote differentiation of the progenitors, FGF2 and EGF are replaced with 20 ng/mL BDNF and 20 ng/mL NT-3 starting at day 25 (with media changes every other day). From day 43 onwards only NM without growth factors is used for medium changes every four days or as needed.

RNA-seq

Total RNA was extracted by RNA purification kit (EZBioscience), and then poly A mRNA was isolated and RNA-seq library was constructed using NEB Next UltraTM RNA Library Prep Kit for Illumina (NEB, Ipswich, MA) according to the instruction manual. The libraries were sequenced on an Illumina HiSeq X Ten platform with 150bp pair-end reads. All reads passed filter were trimmed to remove adaptor sequences and low-quality bases using trim_galore(v0.6.4). Reads were aligned to the GRCh38/hg38 genome reference using STAR (v2.7.5b), and the counts were calculated using featureCounts(v2.0.0). The gene and repeat expression was normalized by transforming raw counts into Transcripts Per Million (TPM). R packages edgeR (v3.34.1) (Robinson et al., 2010) and DESeq2 (v1.32.0) (Love et al., 2014) were applied for differential expression analyses.

QUANTIFICATION AND STATISTICAL ANALYSIS

Data are presented as mean $\pm$ SD, unless otherwise indicated. Differences between 2 groups were analyzed by unpaired t-test, and multiple comparisons between more than 2 groups were analyzed by ordinary one-way ANOVA using Prism 9.0. $p \leq 0.05$ was considered to be significantly different.